Characterizing the Thermal Gradient within Professor Collett's ESR Cryostat

Tobias (Toby) Weissman

Thursday, May 15th, 2025

O Muses! O high genius! now vouchsafe
Your aid! O mind! that all I saw hast kept
Safe in a written record, here thy worth
And eminent endowments come to proof.

The Divine Comedy: II, Dante Alighieri[1]

Abstract

The application of a cryogenic low noise amplifier would be greatly beneficial in the manipulation and use of Molecular Nanomagnets for quantum computing purposes using Electron Spin Resonance. The improvements in the signal to noise ratio would enable a lower dilution and extended relaxation times in addition to the improved data. But, in order to implement such a device, a thorough study of the temperature behavior within the current apparatus must be done. In this thesis we take the initial necessary steps. We acquired and integrated a second thermistor, began studying the thermal gradient within the cryostat, and found areas of future experimentation which should be looked into as we advance with the cryogenic LNA's implementation.

Acknowledgment

I want to thank Lizzy, Danny, Madelini, and, of course, Charles for all the help and support this semester and throughout my time at Hamilton College. I could not have made it without the love and guidance from everyone in the physics department, especially Gordon and Seth, as well as all my friends and number one supporters (and haters) and my girlfriend Claire. It has truly been an awesome, formative time of my life, and I am so grateful for all the kindness and love along the way.

Contents

1 Introduction

Electron Spin Resonance (ESR) is a powerful tool for analysis. It is used for the study of, for example, organic and inorganic radicals, complexes of paramagnetic ions, and triplet states. In the case of Professor Collett's lab, we are using ESR to manipulate Molecular Nanomagnets or MNMs. MNMs are spin systems which can be chemically engineered to have properties desirable of qubits, and thus can serve as an important tool in exploring new quantum computing implementations [2]. Qubits are the fundamental unit of quantum computing just as the binary bit is the fundamental unit of classical computing. MNM can be used as qubits because they can be designed to hold a superposition of states and exhibit entanglement, requirements for quantum computing. For all ESR, and especially our work with MNM and their very quick decoherence times, strong data processing is required. The samples are quite diluted and as such the signals are quite weak so when amplified the data has low signal to noise ratio and thus a high proportionate amount of noise. With the current set up a room temperature amplifier is used, which although successful in amplifying the data, requires large amount of post processing to remove its introduced noise. This has led many, and now us, to look into the use of a cryogenic low noise amplifier, which our ESR experiments are a good candidate for. Cryogenic amplifiers, because of decades of engineering and theory, are able to greatly increase the signal to noise ratio in comparison to their room temperature counterparts. ESR already requires ultra cold temperatures to function and as such allows us to capitalize on the existing machinery to cool the amplifier to the ideal temperature. That is why this has been explored and implemented with great success in Refs. [3] and [4].

My thesis aims at developing a better understanding of the thermal conditions within our current cryostat and in doing so open up the potential for large scale improvements in data processing that would come about from the use of a cryogenic low noise amplifier, like the LNF-LNC0.3_14B by Low Noise Factory which we plan on acquiring. To do so requires the acquisition a new thermistor, preparations for its use, and the study of the temperature within the apparatus in multiple periods of cooling down and heating up. With these results we will be able to better understand what exactly is occurring within the region in which our sample usually sits but also the regions above

it where a future low noise amplifier might be placed.

2 Background

2.1 Electronic Noise

Before we can get into the theory surrounding the application of a cryogenic low noise amplifier, we must first quickly give an introduction to electronic noise and how it is reported and discussed. Electronic noise, like any noise, is problematic when taking data because it can mask or even completely hide the signal. Noise defines the smallest signal power one can detect[5]. Although there are a variety of techniques to remove the noise from recorded data, it is best to reduce the noise from its source as much as possible, especially in situations where the signal to noise ratio is low to begin with. In order to reduce noise it first has to categorized and understood. In scientific and industrial literature when discussing and comparing the noise performance of an electronic device, the noise produced by the device is often reported as the noise temperature of the device. At first glance this seems quite confusing, the temperature of the device and the noise it produces are not directly and linearly related in most cases. By its definition the noise temperature of an electronic device is the power spectral density of the noise it produces in terms of temperature that would produce the same power density by thermal agitation. Thermal agitation is also known as Johnson-Nyquist noise or thermal noise. Johnson-Nyquist noise is generated by the thermal agitation of, most generally, electrons within an electrical conductor. In the simplest way, one can think of the movement of the electrons, due to their temperature, causing voltage fluctuations in the conductor. These fluctuation voltage are the noise which can be picked up on the measuring device. Johnson-Nyquist noise is proportional to the conductor's absolute temperature[5].

To determine the root mean square voltage of thermal noise or Johnson-Nyquist noise one uses the following equation invented by Johnson and Nyquist in the 1920s at Bell Labs, we can derive it the same manner Johnson did with its roots in thermodynamics and Planck's law[5]. First we begin with Planck's black body radiation law. By rearranging Plank's law we get

$$V_{rms} = \sqrt{\frac{4hF_c\Delta f R}{e^{hF_c/k_bT} - 1}}. \tag{1}$$

Then we can approximate assuming $hF_c k_b T$ and using a second order Taylor expansion to approximate the exponential term,

$$V_{rms} = \sqrt{4k_b T R \Delta f}, \tag{2}$$

with $4k_b$ is Boltzmann's constant, T is temperature, R is the resistance of an ideal resistor, and Δf is the frequency range or bandwidth. The voltage, and thus the magnitude of the noise, is directly proportional to the frequency range in question. This means that if measuring noise over a large range, the voltage will he higher, and this is why the power spectral density is used for determining the noise temperature. Additionally, the equation uses the resistance of an ideal resistor like many electronics equations. This is done to simplify the equation, aiding in its purpose of comparison. The ideal resistor acts like most resistor except it is perfectly consistent along all frequencies and because we are interested in power and not voltage, the resistance does not matter. The spectral power density of Johnson-Nyquist noise for a certain temperature can be seen in figure 2.1.

Equation 2 can be rearranged and manipulated for into various equivalent forms easier usage in the following steps,

$$\frac{V_{rms}^2}{R\Delta f} = 4k_b T \tag{3}$$

$$\frac{P}{\Delta f} = 4k_b T \tag{4}$$

$$T = \frac{P}{4k_b \Delta f}. \tag{5}$$

So returning to its purpose, to say an electronic circuit or device has a noise temperature of 75 K for example would be to say the noise it produces has the same power spectral density as a conductor at 75 K due to solely thermal electrical agitations. Although at points confusing, particularly because of the additional focus on the physical temperature of the actual electronic device, noise temperature gives a convenient way to compare the performances of various products as well as generalize their performance without having to get into too much detail about frequency and the nature of the noise. To compare noise performances one would only have to look at the power of the noise over a certain frequency band and calculate the respective noise temperatures of each device.

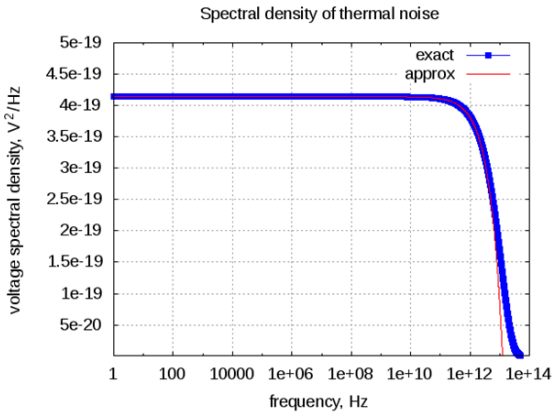

Figure 2.1: Johnson-Nyquist noise power spectral density with its flat voltage spectral density because of its ideal resistor allowing for easy comparison. Taken from Ref.[6].

2.2 Short Introduction to FET Amplifiers

Modern electronics relies on amplification. Early on computers were dependent on vacuum tubes for amplification, but they are large, fragile, expensive, and energy consuming. This has relegated them mostly to the audiophile sphere in the modern day. Nowadays with the advancement of chip manufacturing field-effect transistor or FETs are used often to ampify signals. FETs in their simplest descriptions are essentially valves, either allowing current to flow from source to drain or not dependent on the gate voltage. What leads FETs to be effective amplifiers is that they can exhibit a variability in their "openness" for lack of a better word. once above their cut-off voltage FETs can exhibit almost linear behavior between the input gate voltage and the output current. The ratio of these two values is called the transconductance. for more efficient operation as amplifiers, FETs are often biased, as in the input voltage before the signal is present is raised to a certain level, as to function the most linearly[7]. The relationship between input voltage, output current, and transconductance can be seen in figure 2.2.

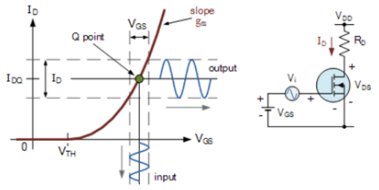

Figure 2.2: Diagram of the operation of a MOSFET amplifier with relationship between input voltage and output current. Taken from Ref.[7].

2.3 History and Theory Behind Cryogenic Low Noise Amplifiers

Although we did not design a low noise amplifier and plan on acquiring a commercially available one, it is pertinent to understand the theory of what goes into the design of an amplifier to better understand our expected improvements to our signal to noise ratio in our Electron Spin Resonance apparatus and to understand the electrical and thermal requirements of such a device. I will be drawing strongly on the work of Marian W. Pospieszalski for the history of their development [8]. Starting in the the 1960s and 70s there was a drive to derive a set of mathematical equations which could model the behavior of amplifiers, allowing for quantitative analysis of the variables and components within the electronic amplifiers as well as a better mathematical understanding of noise at a fundamental level, with the eventual hope of the creation of stronger electronic amplification circuitry with lower noise. This need was at first driven by fields like radio astronomy and deep space communication but the product of these models and improvements have had far reaching consequences, like in our hopeful improvements to the signal processing in our apparatus. Van der Ziel first pioneered in the field with his semi-empirical noise temperature equation for FET amplifiers, which has been improved and iterated on by others [8]. The original equation is,

$$T_{min} \approx T_0 K_f \frac{f}{f_T} \sqrt{g_m (r_g + r_s)} \tag{6}$$

Here, T_0 is the reference temperature (290 K), and K_f is a fitting factor (a parameter ranging roughly from 1.2 to 2.5). The operating frequency f is normalized to the transistor's intrinsic cutoff frequency f_T , while g_m is the transconductance and r_g and r_s denote the parasitic gate

and source resistances. Transconductance is the relationship between the input voltage and the output current, and the parasitic gate and source resistances are unintended resistances that causes undesired current flow. Just in its elementary form the equation gives us parameters to modify and adjust to improve the noise temperature of the device. By postulating relationships between the minimum noise figure and quantities like transconductance, parasitic resistances, and intrinsic capacitances, engineers and scientist could empirically fit and then predict the noise behavior of FET devices, even if the fitting factors themselves did not have an immediately obvious physical meaning[8].

This work was further aided by the iterations of these semi-empirical noise equation. In the new models it was determined that the parasitic resistances of the gate and source only contribute thermal noise. As such they could written as a noise temperature just as discussed earlier with noise performance. This along with a redefinition of the transconductance through equivalent circuits produces the following equation,

$$T_{min} \approx 2\frac{f}{f_t}\sqrt{(r_s + r_g + r_{gs})T_g g_{ds} T_d}. \tag{7}$$

From this equation it became clearer for engineers to find the ways in which to improve the amplifying circuit as well as the relationship to the temperature of the circuit. It is important to note that T_g and T_d are not temperatures, physically, but the noise temperature of those specific component parts, the drain and the gate. From equation 7it can be seen that the cut-off frequency should be maximized which is modeled by

$$f_t = \frac{g_m}{2\pi C_{gs}}, \tag{8}$$

and that the parasitic resistances of the gate and source should be minimized. Because of the redefinition in terms of equivalent circuits, the noise contribution of the resistances r_s, r_g and r_d of this now equivalent circuit are determined by the physical temperature T_a of a chip [8]. This made the relationship between temperature and the expected performance equation in 7 more clear.

These two avenues of improvement were pursued by engineers and scientist leading to mar-

ketable improvements that are still in use today with the low noise amplifier we chose to acquire. For maximization of the cut-off frequency, improvements in technology allowed for the creation of FET's on a smaller scale and of different materials. The materials composition of the FETS and HFETS are often denoted by the elemental composition. Prior, epitaxial GaAs material was used exclusively but in the 70s new materials like GaInAs and in the 90s, particularly important to us, InP HFET were developed [8]. Additionally the lengths of the gate leads were shortened from 1 μm in the 70s to under .1 μm. With the objective in mind to reduce the parasitic resistances, FETs were restructured with "mushroom" or T gates, reducing the drain-to-source separation. Equation 7 also gives a model for which to optimize FET bias, as T_d and f_t are functions of the transistor bias. A simulation based on equation 7 can be seen in figure 2.3. It is important to note the lowered noise temperature dependent on the ambient temperature which can be seen on the distinct lines with 12.5 K having the lowest.

Given these models, engineers were able to rapidly iterate on amplifier designs, settling around the late 90s, with the adoption of InP HFETs. InP HFETs produced nowadays take advantage of all the advancements of the previous models but are less prone to illumination and produce much more repeatable results . HFETs stands for Heterojunction Field Effect Transistors. Unlike traditional FETs, as their name suggests, HFETs are consists of a junction between two hetero material which allows for higher frequencies and better switching properties, which enable our better signal processing once we acquire the LNA. This section serves not as a conclusive history of the design of HFET's, but merely an introduction into the theory that surrounds the design of the HFET we will be using in our apparatus. For a more detailed dive into the history and theory Refs. [8] and [4] provide great analysis.

2.4 Motivating Factors

Before the introduction of any cryogenic low noise amplifier into our ESR apparatus, the temperature conditions within our cryostat chamber, made by Lake Shore Cryotronics as shown in figure 2.6, must be better understood. This is because as discussed in the theory sections,

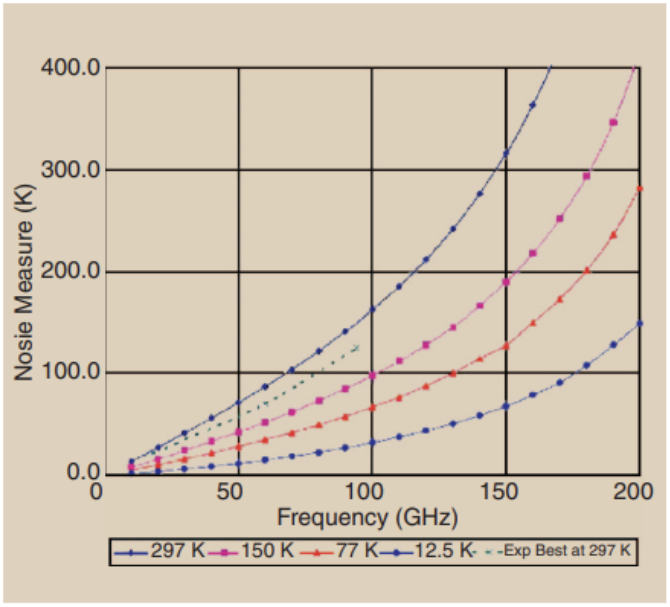

Figure 2.3: HFET modeled noise temperature given the chip temperature as a function of frequency. Taken from Ref. [8]

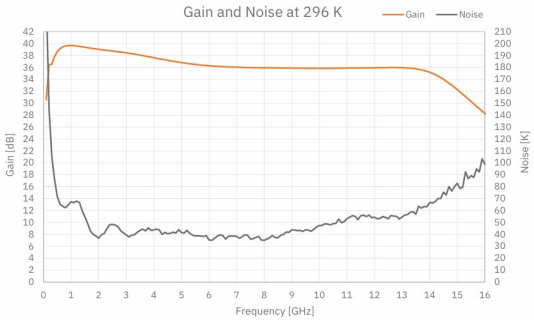

Figure 2.4: Sensitivity of the LNF-LNC0.3_14B at 296K. Taken from Ref. [9].

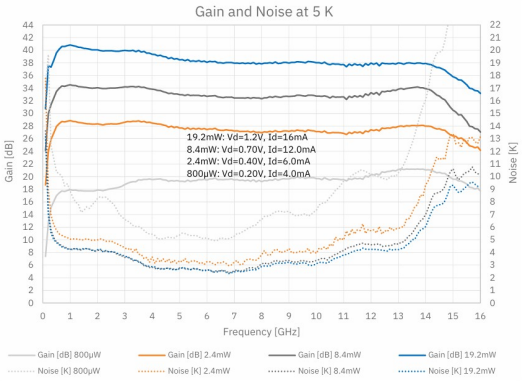

Figure 2.5: Sensitivity of the LNF-LNC0.3_14B at 5K with different amperage. Taken from Ref. [9].

the performance of a LNA , like the LNF-LNC0.3_14B by Low Noise Factory we are acquiring, is dependent on the ambient temperature, as can be seen in figures 2.4 and 2.5. Thus, to understand how in our eventual application our LNA will function, we must know the temperature gradient within the chamber. This is not possible with the original configuration. It its original form, the cryostat had a singular integrated thermometer located at the bottom of the sample tube as can be seen in the diagram of the Janus Cryostat in figure 2.6, circled in red. The integrated temperature sensor has four wires which exit the chamber alongside the heating wires and lead into a Lakeshore Model 335 Temperature Controller. From there the temperature of the chamber is monitored. With our original set up we are able to understand the temperature behavior of a limited but important region of cryostat. With the original thermistor we can monitor our cryostat as it comfortably sits at around 3 K for extended periods of time as well as it drops to just under 1.5 K for short periods of time through the condensing and pumping of helium into the chamber.

The problem is with the singular temperature probe is exactly that, it is singular. There is only a single point for which we know for certain the temperature of and it is not directly of our sample but rather the temperature of the tube. The introduction of a second sensor will help to address this problem through a better understanding of what is going on in the chamber. With the new thermometer we have two goals. The first and short term goal which we achieve in this paper is to use the thermometer get a better understanding of the temperature gradient within the chamber, from the bottom up. As can be seen in figure 2.7 our probe consists of different distinct areas separated by 3d printed baffles. This means that we expect each region to have a different temperature when our apparatus is cooled down. The study of the temperature gradient is beneficial for a better understanding of what is occurring in our cryostat but also necessary for determining the efficacy of placing a LNA within the chamber at a certain baffle level. Each level's temperature can be measured, one at a time, because, unlike the original probe used in the cryostat chamber, the second sensor is free standing and can be moved throughout the chambers and baffles after each cool down and warm up cycle. Our second and long term goal with the new temperature sensor is to permanently attach it to the sample chamber. This will offer us a clearer reading of what exactly the temperature of our sample is, reducing the uncertainty.

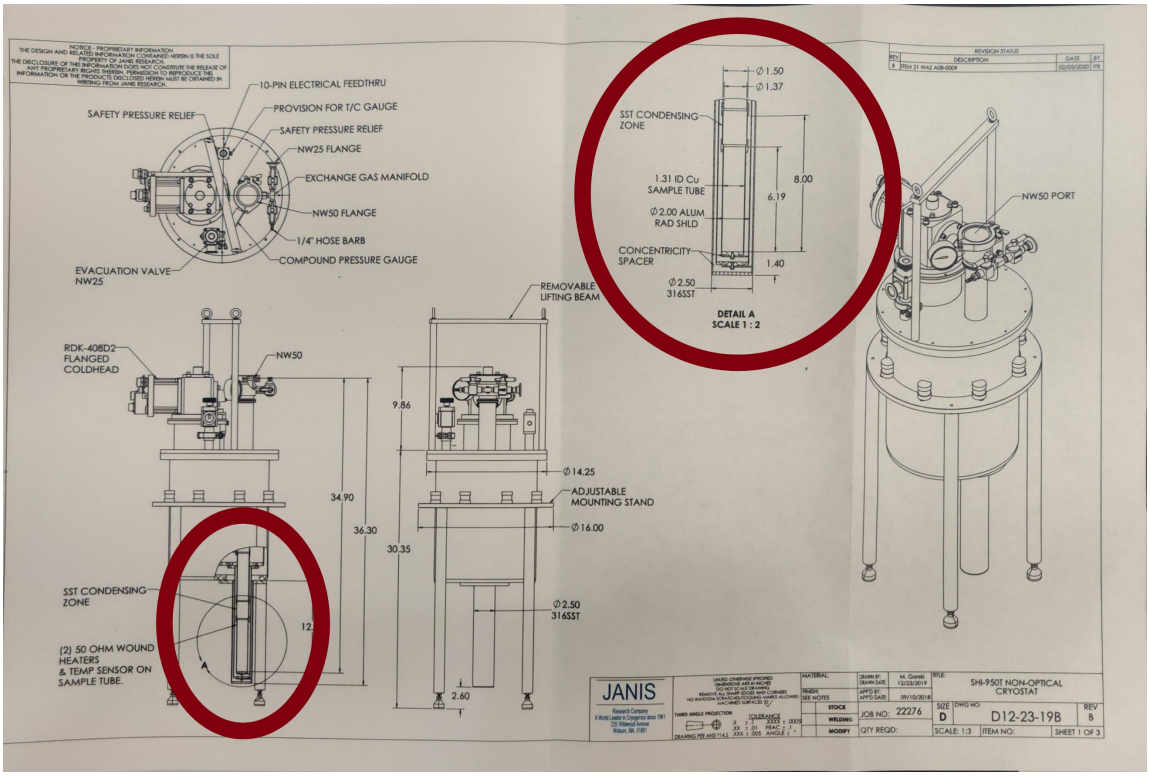

Figure 2.6: Janus provided schematic for the cryostat. The highlighted circle is the part of the chamber where the sample, condescending zone, integrated temperature sensor are located.

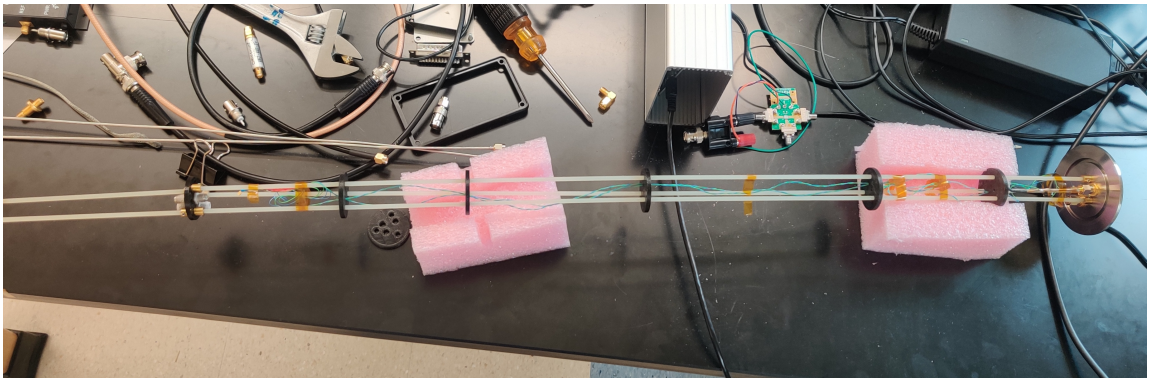

Figure 2.7: Prepared temperature probe with the Cernox® temperature sensor in the second lowest baffle region.

3 Apparatus

As mentioned before our ESR apparatus consists of a Janus SHI-950R Non-optical Cryostat. Attached to the cryostat is a bottle of high-purity helium, a vacuum pump, and an external helium cooling unit, as well as all the electronics necessary for ESR experiments. Through the external cooler it can reach as low as 3 K and with the vacuuming of helium it can reach as low as 1.4 K temporarily. Integrated within the cryostat, as can be seen in 2.6, and connected to a Lake Shore Model 335 Temperature controller is an integrated Cernox®thermistor. Within the cryostat we can insert an interchangeable probe. During normal operation we use a sample probe with a bimodal resonator located at the bottom, but for our temperature experiments we have used a separate test probe. This probe has been striped of a sample chamber but still contains the 3d printed baffles as our other probe. As such, we can assume the temperature gradient within the chamber is quite similar to during our ESR experiments. The equipped test probe can be seen in figure 2.7. It will be described further in detail in section4.2. Each probe consists of a cap with coax connectors on the top. This allows us to seal the chamber with a clamp while allowing for us to have up 4 connections into the chamber.

4 Methods

4.1 Acquiring the thermistor

To satisfy our goals, we had to purchase additional sensors for our apparatus. We decided to acquire from Lake Shore Cryotronics to ensure a seamless integration of the new sensor into our existing apparatus. This is because Lake Shore provides detailed instructions for the sensors they sell which have been tested with the Lakeshore Model 335 Temperature Controller, which we currently use. Lake Shore offers a variety of cryogenic temperature sensors, but we decided to order a Cernox® negative temperature coefficient RTD because of our familiarity of the product, as it is the same type as our existing functioning temperature sensor, and has seamless compatibility with

our temperature controller with no necessary modifications. The thermistor we chose is an RTD, which stands for resistance temperature detectors and has a negative temperature coefficient, which means that the resistance decreases as the temperature increases. The Cernox® sensor come in a variety of product lines with varying temperature ranges and sensitivities. For our apparatus and situation we selected the CX-1050 as our sensor of choice. It offers excellent sensitivity over our desired range of 1.4 K to 300 K, which is the range of our cryostat as can be seen in figure4.1.

The second question with regards to ordering the temperature sensor is in what package do desire it in. The sensor itself is quite small so the size of the complete probe is highly dependent on the selected package. Lake Shore offers a wide range of packages all trading off on: size, thermal response, ease of mounting, lead thermal anchoring, and magnetic composition. Because of our desire for flexibility in placement and no requirement for magnetic composition we selected the SD package for our probe. The SD package consists of a small rectangular prism of dimensions .075 x .0125 x .042 inches made of a sapphire base and alumina body and lid. Its small size and rectangular shape allows for the maneuverability of the sensor within the cryostat for our first goal as well as the easy mounting for when we permanently attach it to the sample probe in its final application. The SD package is ideal for mounting with epoxy. Additionally when ordering, we purchased a calibration for the specific sensor from Lake Shore, this would allow us to input a resistance to temperature map into our temperature controller and expect accurate results. The advertised description by Lake Shore of the SD package can be found in figure 4.2.

4.2 Setting up the temperature sensor

Once the probe was acquired and delivered, it had to be prepared for our apparatus. To prepare it for use, the probe had to be wired and calibrated with our temperature controller, using the provided calibration by Lake Shore. For the wiring of the device, we followed the instructions of the Lake Shore manual regarding the temperature controller. For the ideal performance, the probe which only has two 1 inch golden leads, was split off into 4 different wires, separating the voltage and current sensing wires, this serves to reduce any error due to the resistance of the wires. Because

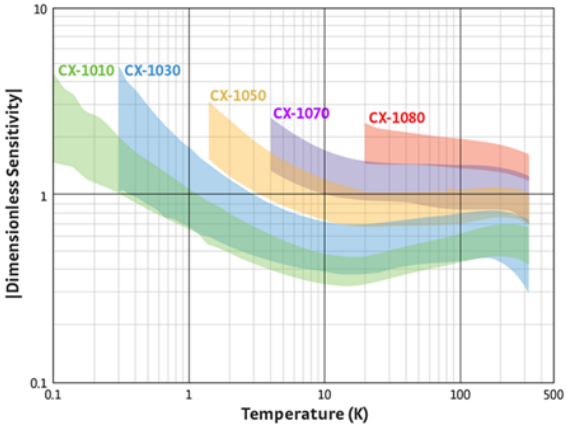

Figure 4.1: Cernox®Sensors' Sensitivities. Taken from Ref. [9]

Figure 4.2: Cernox®SD specifications. The advertised small size and ease of mounted is what motivated our decision to go with the SD package. Taken from Ref. [9].

of our apparatus, two sets of four wires were used to ensure a temperature seal within our cryostat and to require the least amount of modifications. One set is within the chamber and another is outside, always remaining room temperature. The wiring can be seen in figure 2.7. Small gauge wire 26 AWG was used within the chamber for flexibility without the worry of too much thermal conduction. Thermal conduction would be an issue because if the sensor was in the lower, colder baffle region while the wires traveled through the higher baffles regions to the exit, heat could travel down the thermally conductive wires and raise the temperature of the probe, obfuscating our results. The voltage wires and the current wires were twisted together separately to reduce interference. The ends were terminated onto male coax connections. This was done to allow for easy disconnecting as well as compatibility with our original set up. Two sets of twisted pairs exited the chamber, this time using larger gauge wire, 22 AWG, and the connections were terminated to two male coax connections as well as the lid contains two male to male coax connections. The connections at the end of our sensor wires allows us to easily connect them through the cap of our cryostat as can be seen in figure 4.3. With regards to the end of the external wires, they were terminated in a male 6 DIN connector according to Lake Shore's instructions as can be seen in figure 4.6. This connector was used to plug into port B in the back of the temperature controller, see figure 4.6.

For the purpose of mapping the temperature gradient of our chamber, an old sample probe was used, to allow for the continued use of our other probe for experiments when the temperature experiments are not occurring. The separate probe allows us to weave the temperature sensor down through the baffles which segregate parts of the chamber, without interference. For the process of taking the temperature of a certain baffle region we first place the sensor within the area we want, in between the baffles as to get the general temperature of the area and secure it using Kaptontape as seen in figure 4.7. We then pull the small interior wires taut and loop them around in the second highest baffle region before securing them with more Kapton tape. It is vital to secure all the wires and make sure none are outside the diameter of the baffles because then they could be caught when inserting the probe into the cryostat. More tape was sometimes needed in the other regions to insure there would be no snaring.

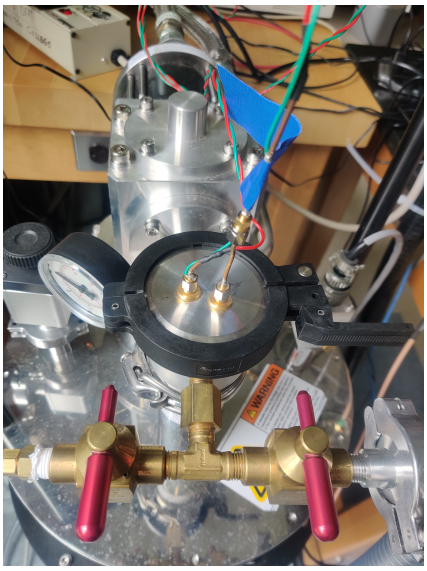

Figure 4.3: The top of the cryostat when the temperature probe is within the chamber. The two male coax connections at the top allow for quick connection and flexibility. The thicker twisted pairs are also visible.

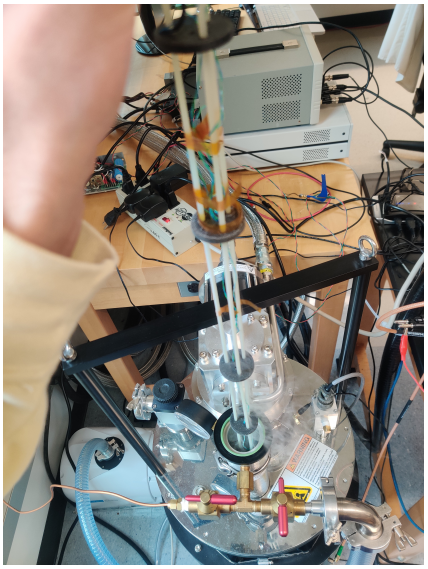

Figure 4.4: The removal of the temperature probe during a "cold swap" back to the sample probe, which will be described in more detail in section 4.3. The left valve controls the flow of helium which can be seen to be open during the swap.

Figure 4.5: Wired up 6 DIN male connector.

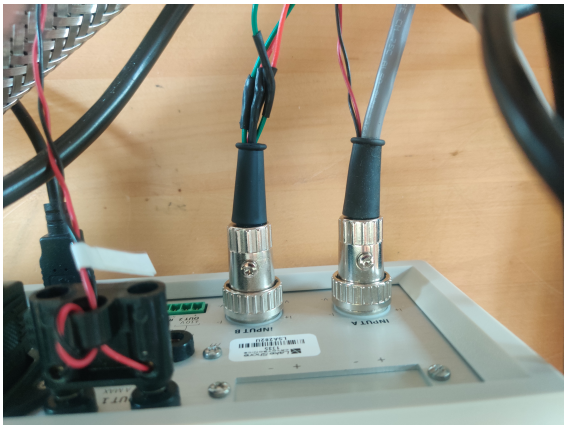

Figure 4.6: Plugged in DIN connection into input B of our Lake Shore Model 335 Temperature Controller. Input A is the integrated thermistor.

Figure 4.7: The placement of the movable thermistor in the second baffle region, with a ruler as a fiducial.

4.3 Taking temperature measurements

Once our probe is set up we can begin the process of inserting it into the cryostat. There are two processes when switching to our temperature probe, a "cold swap" or a full restart, depending on the state and usage of the apparatus before hand. The standard procedure is starting from a completely room temperature system. To begin we remove the sample probe or the blank probe and insert our temperature probe with the thermistor attached at a certain baffle level. Once in we seal the chamber and flush and evacuate the tube a couple times using a vacuum and a bottle of high-purity helium. Then when satisfied with the helium content within the chamber, we close off all the valves and begin the process of chilling the cryostat.

If we are using the cryostat prior to the use of the temperature probe we preform what we call a "cold swap." The cold swap consists of raising the sample probe in the cryostat to around 250 K, using the internal heaters or just by turning the cooling mechanism off and waiting. We then turn on the helium flow into the chamber and prepare our temperature probe for insertion. We then uncap the top of the chamber, and we delicately remove the probe, trying to disturb the gasses as little as possible to maintain a high level of helium within as to not require the pumping and vacuuming of the chamber as with a warm start. It is important to not introduce outside air as the

varaities of boiling points can lead to issues during cool down. We then quickly but carefully insert our temperature probe and latch the lid. During this operation helium is flowing into the chamber to reduce the introduction of outside gasses. We then follow the standard procedure and lower the temperature using the external chiller.

If we desire to reach the temperature of 1.4 K we continue to flow helium into the chamber as it is being chilled, allowing for the collection of liquid helium at the bottom of the chamber, submersing our probe head and lower baffles. This by its own will not lower the temperature of the chamber dramatically, unless there is a lack of transfer gas in which the "cold" can be transferred from the condensing zone to the rest of the chamber. The arrangement of the condensing zone and the sample tube and integrated thermometer can be seen in figure 2.6. When our standard low temperature of around 3 K is reached we can shut off the flow of helium, we then take a measurement using the temperature controller and then begin pumping. This will decrease the pressure within, lowering the boiling point of helium and thus begin removing heat from the chamber. Using this technique we can comfortably reach around 1.4 K.

Throughout this process, the temperature is reported our Lake Shore Model 335 Temperature Controller for both temperature sensors, the one integrated within the apparatus and our new movable one. By manually taking the temperature of both and the time we can get a better understanding of the gradient within the chamber as well as a new understanding of the rate at which the chamber heats and cools. Limited for time, the majority of the study of the temperature gradient was done in during the extra cool down process from 3 K to 1.4 K as this is the state our apparatus is in during our electron spin resonance experiments.

4.4 Heat up measurements

To better understand the temperature behavior inside the chamber we also conducted experiments when heating the chamber with the integrated heating coils as can be seen in figure 2.6. This was done through the connected PC which would enable a ramped heating curve as to keep a constant temperature increase based on the integrated thermistor. Any build up of gasses from

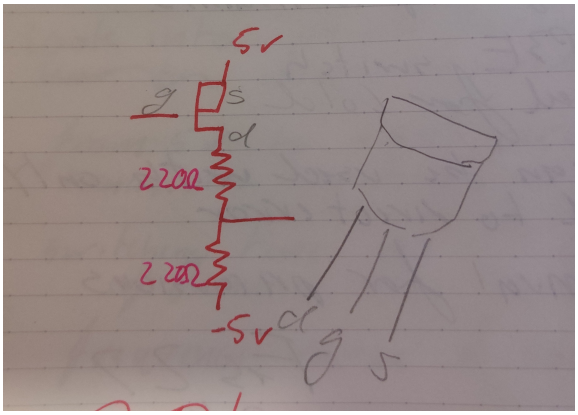

Figure 4.8: Circuit diagram of necessary inversion of 5v signal to -5v signal.

the raising temperature would off-gas through a pressure release valve at the top of our cryostat.

4.5 Switching Electronics

Tangential to the temperature experiments, work was done on preparing and investigating the circuitry required to operate the LNA were are looking to acquire. The LNF-LNC0.3_14B, unlike the other electronics currently used in our ESR apparatus, requires negative signaling voltage. Our current FPGA does not support negative voltage so a small switching circuit will be required. A simple MOSFET circuit was designed and quickly implemented on a bread board. The circuit diagram is shown in figure4.8. At first the circuit was made with high resistance resistors but they were later changed for 220Ω resistors to enable faster switching.

In its final implementation this circuit will be printed on a PCB. This will then interface between our existing controlling electronics and the PCB mounted cryogenic signal switches designed by students at Amherst that will go between the LNA and the resonator. .

Lowest Baffle Temperature Drop Measurement

Time Pumping	**U T (K)**	**I T(K)**	**time**	**ΔU**	**δU C**	**ΔI**	**δI C**	**Δt(s)**
0:00:00	3.319	3.321	10:18:26					
0:05:01	2.149	2.130	10:23:27	-1.170	-1.166	-1.191	-1.187	301
0:10:02	1.862	1.848	10:28:28	-0.287	-0.286	-0.282	-0.281	301
0:15:27	1.749	1.741	10:33:53	-0.113	-0.104	-0.107	-0.099	325
0:20:02	1.728	1.723	10:38:28	-0.021	-0.023	-0.018	-0.020	275
0:25:14	1.720	1.715	10:43:40	-0.008	-0.008	-0.008	-0.008	312
0:30:11	1.713	1.709	10:48:37	-0.007	-0.007	-0.006	-0.006	297
0:35:01	1.706	1.703	10:53:27	-0.007	-0.007	-0.006	-0.006	290
0:40:12	1.671	1.667	10:58:38	-0.035	-0.034	-0.036	-0.035	311
0:44:57	1.633	1.624	11:03:23	-0.038	-0.040	-0.043	-0.045	285
0:50:02	1.542	1.531	11:08:28	-0.091	-0.090	-0.093	-0.091	305
0:55:09	1.485	1.477	11:13:35	-0.057	-0.056	-0.054	-0.053	307
1:00:29	1.454	1.450	11:18:55	-0.031	-0.029	-0.027	-0.025	320
1:04:52	1.446	1.443	11:23:18	-0.008	-0.009	-0.007	-0.008	263
1:10:20	1.441	1.439	11:28:46	-0.005	-0.005	-0.004	-0.004	328
1:14:54	1.439	1.438	11:33:20	-0.002	-0.002	-0.001	-0.001	274
1:20:24	1.436	1.435	11:38:50	-0.003	-0.003	-0.003	-0.003	330
1:24:56	1.434	1.434	11:43:22	-0.002	-0.002	-0.001	-0.001	272

Table 1: Data collected when we began pumping with the U thermistor, the movable new thermistor, in the lowest baffle region. I is the integrated thermistor. Time pumping is the time since the engagement of the pumping process. U T and I T are the reported temperature in kelvin. Time is the recorded time of the measurement. ΔU and ΔI are the change in temperature from the previous measurement, and δU C and δI C are the corrected changes in temperature to a standardized 5 minutes, with the units K/5min. Δtime(s) is the time between measurements in seconds.

5 Results

Although limited by time, valuable data was collected to begin the characterization of the temperature gradient within the cryostat. In all the graphs and tables the inside, integrated thermometer is labeled I Thermistor, and the outside, movable thermometer is labeled U Thermistor. With regard to the location of the U thermistor: the lowest baffle region is the coldest and deepest in the cryostat below all the 3d printed baffles, the second baffle region seen in figure 2.7 is the second lowest, and the third baffle region is the third lowest. For all the baffle regions the sensor was located around equidistant from each baffle as evidenced in figure 4.7.

Table 1 and figures 5.1 and 5.2 are a result of our experiment with the U thermistor in the lowest baffle region which is submerged in liquid helium. Alongside the recorded temperature of

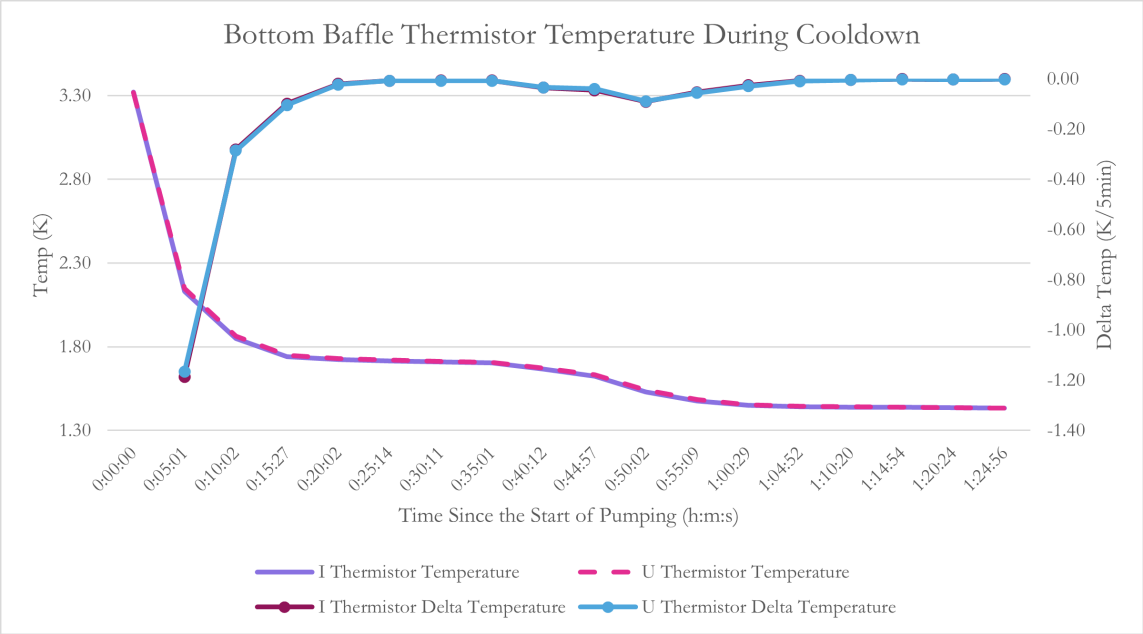

Figure 5.1: Double axes graph for the lowest baffle cool down of the temperature U and I with the axis on the left and the δU and δI with their axis on the right

each probe, in kelvin, and the time of measurement, is the calculated changes. This is done to allow us to see the trends and grant us a better understanding of how and at what rate the temperature is changing within the chamber. The table, and all subsequent tables except 4, contain ΔU and ΔI as well as δU C and δI C. The first set is merely the change in temperature between the last measurement. With the second δ we are correcting and standardizing for the period of 5 minutes, and as such they are marked with a C. Without this calculation the rates of change would be incomparable. There were standardized to the period of 5 minutes as that was the average period when first taking data, and the large period gives an understandable unit with which to understand the temperature changes in the chamber. For table1 the difference in ΔU and ΔI to δU C and δI C are small but with the others experiments with more varied times between measurements the standardization becomes more important.

With the heat up measurements we are following the procedure outlined in section 4.4. The temperature reading do not start at our lowest values because prior we had let the cryostat heat

Lowest Baffle Temperature Heat Up Measurement

Time H	**U T (K)**	**I T(K)**	**Time**	**ΔU**	**H%**	**δU C**	**ΔI**	**δI C**	**Δt(s)**
0:00:00	35.047	43.004	16:10:02		31				
0:02:44	57.554	70.355	16:12:46	22.507	43	41.171	27.351	50.032	164
0:03:51	64.134	81.696	16:13:53	6.580	46	29.463	11.341	50.781	67
0:04:50	73.954	91.570	16:14:52	9.820	49	49.932	9.874	50.207	59
0:05:50	78.325	101.540	16:15:52	4.371	51	21.855	9.970	49.850	60
0:07:40	92.287	119.860	16:17:42	13.962	56	38.078	18.320	49.964	110
0:10:10	110.990	144.880	16:20:12	18.703	61	37.406	25.020	50.040	150
0:11:47	125.440	161.030	16:21:49	14.450	64	44.691	16.150	49.948	97
0:13:46	140.480	180.950	16:23:48	15.040	67	37.916	19.920	50.218	119
0:16:31	163.700	208.360	16:26:33	23.220	72	42.218	27.410	49.836	165
0:18:23	176.600	227.070	16:28:25	12.900	74	34.554	18.710	50.116	112
0:20:33	195.460	248.860	16:30:35	18.860	76	43.523	21.790	50.285	130
0:23:10	222.240	274.910	16:33:12	26.780	78	51.172	26.050	49.777	157
0:24:16	230.350	285.990	16:34:18	8.110	79	36.864	11.080	50.364	66
0:25:06	236.000	291.030	16:35:08	5.650	66	33.900	5.040	30.240	50
0:26:48	246.950	290.410	16:36:50	10.950	58	32.206	-0.620	-1.824	102
0:29:00	253.870	290.060	16:39:02	6.920	58	15.727	-0.350	-0.795	132
0:32:10	255.560	290.010	16:42:12	1.690	57	2.668	-0.050	-0.079	190
0:33:46	255.320	290.030	16:43:48	-0.240	56	-0.750	0.020	0.062	96

Table 2: This is the results of a heating experiment with the U thermistor in the lowest baffle region, in which the heaters were applied on a curve to linearly raise the temperature. Time H is the time from which the heating coils were turned on. H% is the percentage of the heating unit's heating capacity being used as reported by the temperature controller. The other variables are the same as table 1.

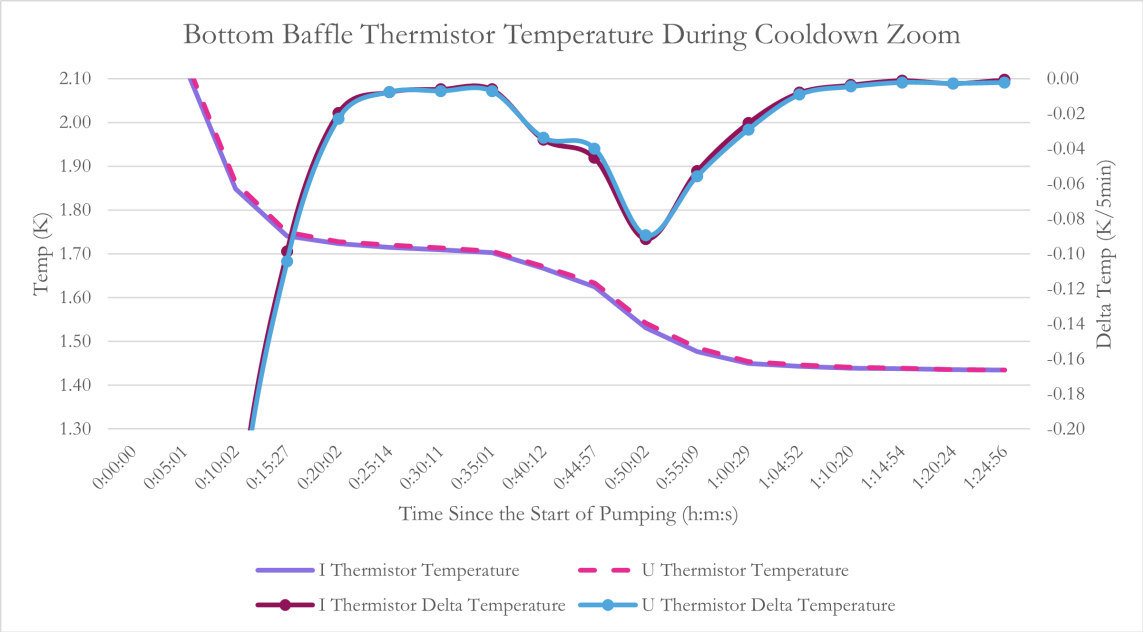

Figure 5.2: The same data as figure 5.1 but zoomed in to the range 1.3-2.1 K and 0.00-0.20 K/5min on the y axes.

up naturally as the cooling apparatus was disengaged. It is important to note that our heating script goes until the I thermistor reaches 290 K and the rate is determined to maintain a constant change in I thermistor temperature until then. With the heat up measurements we also include what percentage of integrated heating coil's heating capacity is being used as reported by the temperature controller. Additionally when taking the heat up measurements it was noted that at the high temperatures above 250 K there was an observed extreme variability in the U thermistor temperature reading of up to $\pm$ 4 K.

In the measurements of the second baffle level the process was much of the same, recorded in 3 and figures 5.4 and 5.5. Unlike with the lowest baffle, we observed the divergence of the two temperature readings. The conclusions we can make will be discussed in the next section. No heat up measurements were made with the second baffle placement because we concluded the results would be similar to with the first baffle measurements.

In our final test with the U thermistor in its highest location yet of the third baffle region, we

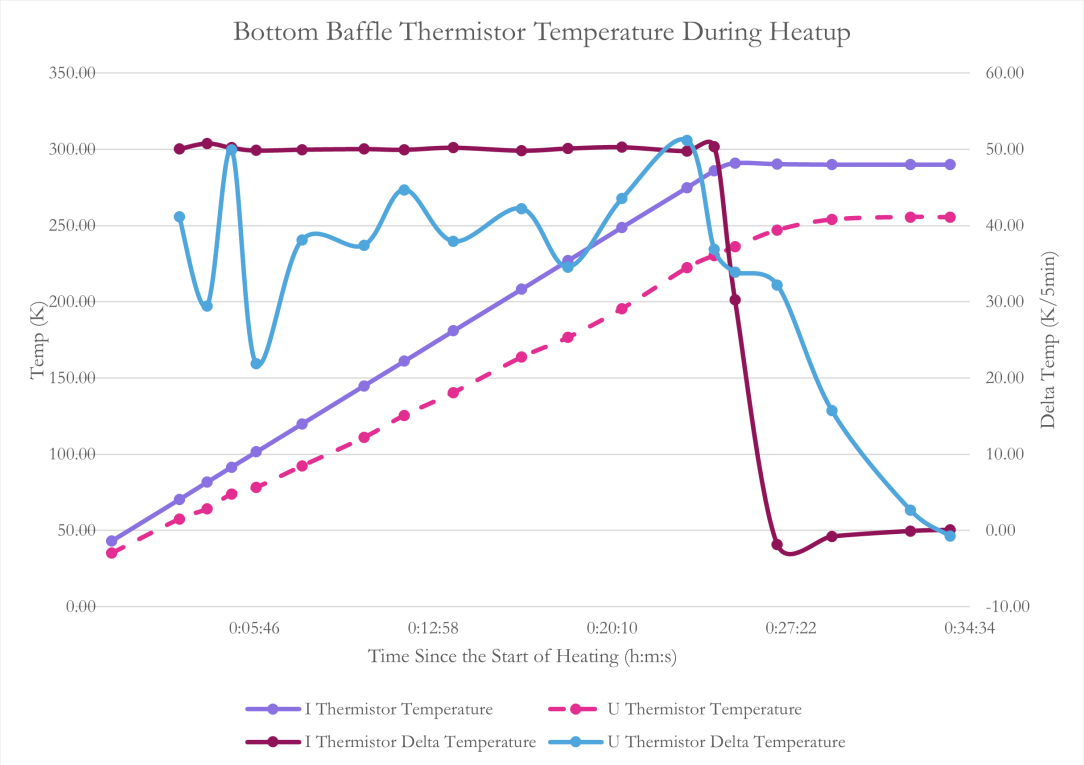

Figure 5.3: Double axes graph of the heat up process with the U thermistor in the bottom baffle region. This is with the application of a constant δI temperature increase with a variable heat%.

Second Baffle Temperature Drop Measurement

Time Pumping	**U T (K)**	**I T(K)**	**time**	**ΔU**	**δU C**	**ΔI**	**δI C**	**Δt(s)**
0:00:00	3.447	3.424	18:34:38					
0:00:30	2.523	2.504	18:35:08	-0.924	-9.240	-0.920	-9.200	30
0:00:56	2.166	2.146	18:35:34	-0.357	-4.119	-0.358	-4.131	26
0:01:20	1.976	1.966	18:35:58	-0.190	-2.375	-0.180	-2.250	24
0:02:03	1.887	1.747	18:36:41	-0.089	-0.621	-0.219	-1.528	43
0:02:34	2.052	1.612	18:37:12	0.165	1.597	-0.135	-1.306	31
0:03:04	2.218	1.506	18:37:42	0.166	1.660	-0.106	-1.060	30
0:03:48	2.407	1.431	18:38:26	0.189	1.289	-0.075	-0.511	44
0:04:30	2.611	1.402	18:39:08	0.204	1.457	-0.029	-0.207	42
0:05:23	2.720	1.389	18:40:01	0.109	0.617	-0.013	-0.074	53
0:08:23	2.796	1.385	18:43:01	0.076	0.127	-0.004	-0.007	180
0:11:53	2.845	1.387	18:46:31	0.049	0.070	0.002	0.003	210
0:16:13	2.873	1.389	18:50:51	0.028	0.032	0.002	0.003	260

Table 3: Data collected when we began pumping with the U thermistor in the second lowest baffle as can be seen in figure 2.7. The variables are the same as table 1.

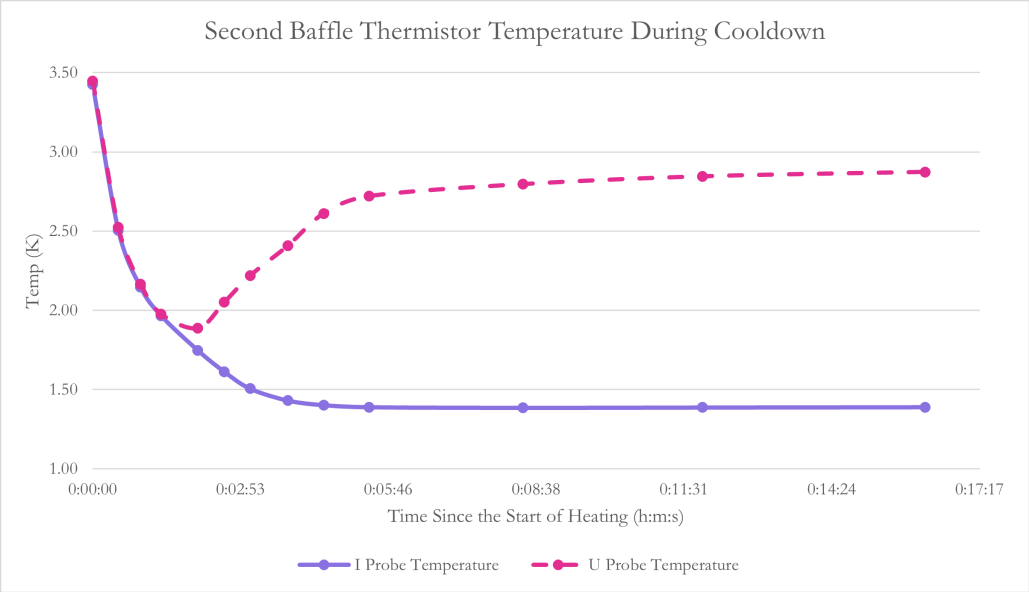

Figure 5.4: The cool down process with the U thermistor in the second baffle without the derivatives for simplicity sake. Here we see different behavior and a difference between the U thermistor and I thermistor readings.

Third Baffle Temperature

Time Pumping	**U T (K)**	**I T(K)**	**time**
0:00:00	8.903	6.425	11:39:53
0:12:01	6.477	4.332	11:51:54

Table 4: Small data collection of the U thermistor in the third baffle region.

were unable to complete a full cool down like the other two runs. This was due to a lack of helium and the unsatisfactory temperature we were able to achieve without the pumping of helium. The first data point is a point of equilibrium taken after 12 hours of cooling. It is not as cold as expected because of the low pressure within the chamber from a lack of helium. After the data point was recorded, some helium was introduced into the chamber and after half an hour the second data point was taken after it was seen to have settled at its temperature.

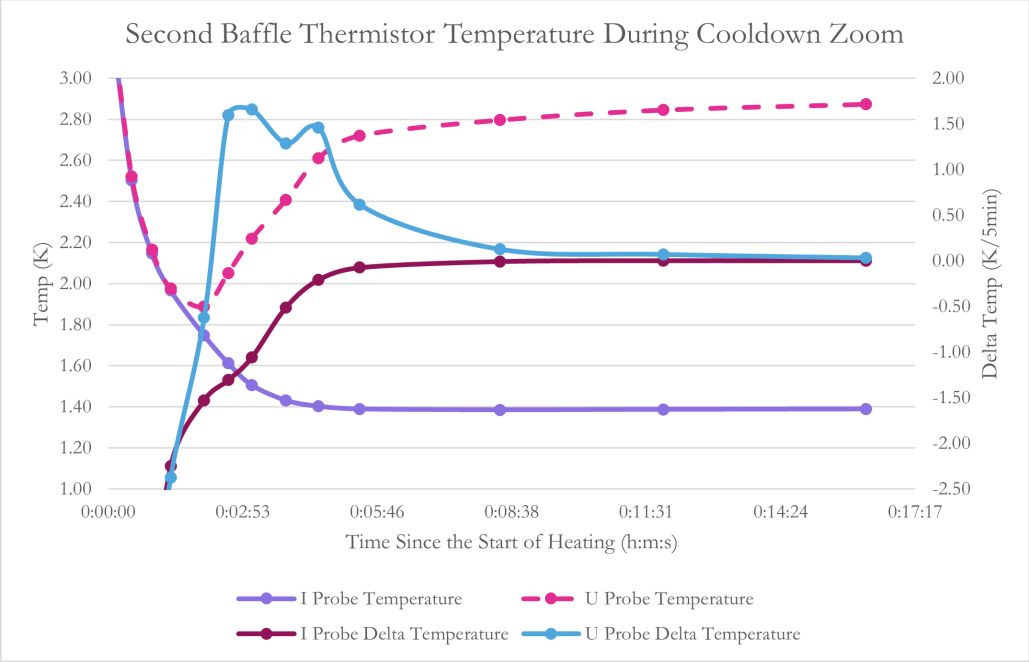

Figure 5.5: The same cool down process of figure 5.4 but with the inclusion of the derivatives and zoomed in. Here we see the divergence of the derivatives which leads to the split in temperature readings.

6 Discussion

With our results we can make some conclusions regarding the temperature behavior in the cryostat and the gradient within. With regards to the first experiment with the U thermistor in the lowest baffles, the concurrence of the two thermistor results can give us confidence in the temperature uniformity within the area around the sample chamber during cool down. As clearly seen in figure 5.2, as well as in table 1, the reported temperatures of both the U and I thermometers are within a few one hundredths of a degree. This also gives us confidence in the the thermistors themselves. The similarity of their results and the temperature at which it occurs also confirms that the bottom chamber is filled with liquid helium during our experiment up to at minimum the level of the U thermistor.

The heat up procedure and data in table 2, gives us a better clue to the proximity of the I thermistor and the heating element. The rest of the chamber is colder, as reported with the U thermistor and seen in the figure 5.3, than the I thermistor measurement. This requires further study and can be done when the long term goal of attaching the U thermistor to the the sample itself is conducted, but the difference in temperature does suggest a certain disconnect or at least lag between the reading of the integrated I thermistor and the temperature of the sample.

Our second experiment with the U thermistor in the second baffle region provides us with more conclusions and confirms our original thoughts. The divergence of the temperatures, unlike that in figure 5.2, demonstrates the importance of the liquid helium level in the temperature of the regions of the cryostat. In the early moments of the cool down process, illustrated in figures 5.4 and 5.5, the temperatures are the same, suggesting that both thermistors are in contact with liquid helium. But, as the liquid helium boils, the level falls, and the temperature decreases, we see the temperatures diverge. With this divergence we can conclude that the U thermistor loses contact with the liquid helium, and as such the temperature rises. For the first time we see a clear stratification of the temperatures within the chamber. The behavior after the initial separation where the changes in temperatures approach zero support this conclusion. Even in the second baffle region there is a distinct stable temperature difference if the liquid helium level is low enough.

Our third experiment, limited by extenuating circumstances, confirms what our second experiment suggested. As can be seen in table 4, there is a clear stratification of temperature. Further experiments should be conducted to measure the temperature as the chamber is cooled down to 1.4 K ,but the preliminary results suggest the possibility of the LNA's placement in this region, as it its not at risk of being in contact with liquid helium as we saw in the second baffle, and, as such, might maintain a more consistent temperature throughout the experiment, independent from the level of helium. In the course of the third experiment we also confirmed the variability of our apparatus, which might prove problematic for fully understanding the future performance of our low noise amplifier.

7 Conclusion

With our results we can continue progressing into the implementation of a cryogenic low noise amplifier, like the LNF-LNC0.3_14B we have been interested in. Our experiment has confirmed our suspicions of the temperature behavior within the cryostat. We have confirmed the presence and importance of liquid helium within the chamber and are now more aware of the levels it can reach and its effect on the temperature of the sample but also the subsequent baffle areas above it. Additionally, the convergence of our temperature readings, between the integrated thermistor and the movable, newly acquired thermistor when in the lowest baffle region, has confirmed the accuracy of our original apparatus as well as reaffirm our confidence in the integrated thermistor having a good reading of the temperature of the sample when in the cool down to 1.4 K and during its time there.

While in their convergence during the cool down period has confirmed the integrated thermistors reliability during cool down and periods of stable temperature, the divergence during the the heat up process and use of the heating coils has revealed a thermal disconnect between the thermistor and the bottom baffle region where the sample would sit. This should not be an issue for our current other experiments with the apparatus, as they all occur during stable temperature periods where the temperature in the bottom baffle region can stabilize, as seen in figure 5.2 with the continuity between readings of the thermistors, but it is something that should be looked into in the future, particularly when the second thermistor is attached to the sample.

Lastly our final, short experiment with the thermistor in the third baffle has given us a better understanding of the gradient, but in the process has revealed the variability of our apparatus. Depending on the conditions, like the amount of helium within the chamber, the temperature of the bottom region as well as all the up the cryostat will be different, affecting in the future the signal to noise performance of our low noise amplifier. This issue should be looked to further along with the placement of the thermistor in all 4 remaining baffle regions of the cryostat to paint a full picture of the temperature gradient.

In conclusion, the work outlined in this paper has further prepared us for subsequent iterations

of our apparatus which will enable better, more precise ESR experimentation. Our testing has confirmed the viability of a future implementation of a cryogenic low noise amplifier and shown us a look within the chamber, giving us a better understanding of what is occurring when we cool down our sample. At the same time is has shown us areas of interest for future study and, with slight modifications, will permanently improve our set up once the thermistor is attached to the sample. With this work and our work with the preliminary electronic controls for a future amplifier, in coordination with Amherst, we are many steps closer to the amplifier's implementation and its major improvements we expect.

References

1. Alighieri, D. *The Divine Comedy* (1321).
2. Jones, P. *Monomodal and Bimodal Loop Gap Resonator Design for Molecular Nanomagnet Characterization* 2024.
3. Mantas Šimenas, e. a. A sensitivity leap for X-band EPR using a probehead with a cryogenic preamplifier. *Journal of Magnetic Resonance 322* (2020).
4. Styles, P. & Soffe, N. A High-Resolution NMR Probe in Which the Coil and Preamplifier Are Cooled with Liquid Helium*. *Journal of Magnetic Resonance 60, 397-404* (1984).
5. Rouphael, T. J. *Wireless Receiver Architectures and Design: Antennas, RF, Synthesizers, Mixed Signal, and Digital Signal Processing* (Academic Press, 2015).
6. Sankar, K. *Thermal Noise and AWGN* https://dsplog.com/2012/03/25/thermal-noise-awgn/. 2012.
7. *Electronics Tutorials: MOSFET Amplifier* https://www.electronics-tutorials.ws/amplifier/mosfet-amplifier.html.
8. Pospieszalsk, M. W. Extremely Low-Noise Amplification with Cryogenic FETs and HFETs: 1970-2004. *IEEE Microwave Magazine* (2005).
9. *Lake Shore Cryotronics: Cernox Sensors* https://www.lakeshore.com/products/categories/overview/temperature-products/cryogenic-temperature-sensors/cernox.